arXiv:2111.11012v1 [physics.plasm-ph] 22 Nov 2021

Brilliant circularly polarized γ-ray sources via single-shot laser plasma interaction

Yu Wang,[1,*] Mamutjan Ababekri,[1,*] Feng Wan,[1,†] Qian Zhao,[1] Chong Lv,[2] Xue-Guang Ren,[1] Zhong-Feng Xu,[1] Yong-Tao Zhao,[1] and Jian-Xing Li[1]

[1]*Ministry of Education Key Laboratory for Nonequilibrium Synthesis and Modulation of Condensed Matter, Shaanxi Province Key Laboratory of Quantum Information and Quantum Optoelectronic Devices, School of Physics, Xi'an Jiaotong University, Xi'an 710049, China*

[2]*Department of Nuclear Physics, China Institute of Atomic Energy, P. O. Box 275(7), Beijing 102413, China*

(Dated: November 23, 2021)

Circularly polarized (CP) γ-ray sources are versatile for broad applications in nuclear physics, high-energy physics and astrophysics. The laser-plasma based particle accelerators provide accessibility for much higher flux γ-ray sources than conventional approaches, in which, however, the circular polarization properties of emitted γ-photons are used to be neglected. In this letter, we show that brilliant CP γ-ray beams can be generated via the combination of laser plasma wakefield acceleration and plasma mirror techniques. In weakly nonlinear Compton scattering scheme with moderate laser intensities, the helicity of the driving laser can be transferred to the emitted γ-photons, and their average polarization degree can reach about $\sim 37\%$ (21%) with a peak brilliance of $\gtrsim 10^{21}$ photons/(s $\cdot$ mm$^2\cdot$ mrad$^2\cdot$ 0.1% BW) around 1 MeV (100 MeV). Moreover, our proposed method is easily feasible and robust with respect to the laser and plasma parameters.

The polarization property of the γ-rays is of great significance to reveal the emission mechanisms in the pulsar [1, 2], magetars and other galactic objects [3]. As an essential tool, γ-ray beams can be used in researches of nuclear physics [4, 5], high-energy physics [6], industrial applications of medical imaging [7] and object tomography, etc. In particular, circularly polarized (CP) ones have broad applications in, for instances, the generation of longitudinally-polarized positron beams [8, 9], polarization-dependent photo-fission of nucleus in the giant dipole resonance [10] and photo-production of mesons [11]. Conventionally, highly polarized photons can be generated via free electron laser (FEL), Thomson and Compton scattering, bremsstrahlung and synchrotron radiation [12]. However, FEL can only deliver X-ray photons of tens of keV, and the peak brilliance and flux of other high-energy γ-ray sources are normally limited by the scattering probabilities and flux of the driving electron beam. For instance, the peak flux of state-of-the-art High Intensity Gamma-ray Source (HIγS) [5] is about 10^{10} photons$\cdot$s^{-1} around 10 MeV with beam diameter of $D \simeq 12$ mm. Recently, rapid developments of ultra-short ultra-intense laser technologies [13, 14] have promoted high-brilliance laser-plasma based particle [15, 16] and radiation sources [17–19]. When multi-PW lasers interacting with plasmas, MeV-GeV γ-photons can be produced with ultrahigh brilliance of 10^{25}-10^{27} photons/(s $\cdot$ mm^2 $\cdot$ mrad^2 $\cdot$ 0.1%BW) [20–22]. However, these produced γ-photons are either unpolarized or only linearly polarized. And all-optical CP γ-ray beams can be generated via multi-PW laser pulses colliding with high-energy longitudinally spin-polarized electron beams in strongly nonlinear Compton scattering [11, 23], which faces potential difficulties of spatial and temporal synchronization. Thus, efficient generation of brilliant CP γ-ray beam is still a great challenge.

In this Letter, we put forward an efficient all-optical method for generating brilliant CP γ-ray beams via single-shot laser plasma interaction. See the interaction scenario in Fig. 1, which is similar to the setup in Ref. [24], however, here we take into account the helicity transfer in the laser plasma interaction. A moderately intense CP laser incidents into a gas plasma and drives the laser plasma wakefield acceleration (LWFA) to generate high-energy electrons. The CP driving laser pulse is then reflected by the plasma mirror and further collides with accelerated electrons to emit CP γ-photons via weakly nonlinear Compton scattering ($e + n\omega_L \rightarrow e' + \omega_\gamma$). Here we find that the helicities of emitted γ-photons in the low-energy regime is mainly associated with those of the driving laser photons. While, for high-energy γ-photons, due to multi-photon absorption, the average helicity will saturate to a constant for unpolarized eletrons or linearly depend on the energies of emitted photons for polarized electrons; see more details in Fig. 3. (By contrast, in strongly nonlinear Compton scattering the circular polarization of emitted γ-photon is determined by the electron helicity [11].) With a moderately intense CP laser, CP γ-photon beams with brilliance of $\gtrsim 10^{21}$ photons/(s $\cdot$ mm^2 $\cdot$ mrad^2 $\cdot$ 0.1%BW) can be generated with polarization degree of $\simeq 37\%$; see more details in Fig. 2. Moreover, the proposed method is robust with respect to the laser and plasma parameters; see more details in Fig. 4.

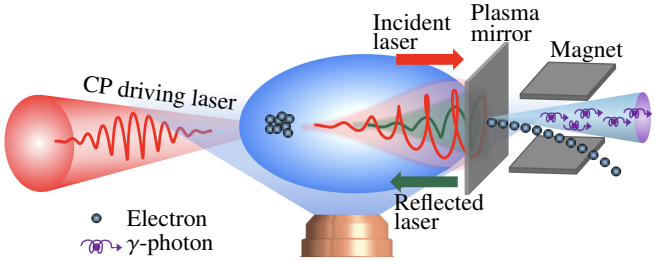


FIG. 1. Interaction scenario for all-optical generation of brilliant CP γ-ray beam via single-shot laser plasma interaction.

In our simulations, we use three-dimensional (3D) particle-

* These authors have contributed equally to this work.
† wanfeng@xjtu.edu.cn

in-cell (PIC) code EPOCH [25] to simulate the LWFA process, and the Monte Carlo code CAIN [11, 26] to simulate the weakly nonlinear Compton scattering process. As an example, we employ a right-hand CP laser pulse (helicity $h_L = -1$) propagating along z direction with wavelength $\lambda_0 = 0.8\ \mu$m, normalized intensity $a_0 \equiv eE_{\rm rms}/m_e c\omega_L = 2.8$ [corresponding peak intensity $I_0 \approx 2.74\times10^{18} a_0^2 (1\ \mu{\rm m}/\lambda_0)^2\ {\rm W/cm^2} \approx 3.46\times10^{19}\ {\rm W/cm^2}$], and transverse Gaussian profile with focal radius $w_0 = 11.5\ \mu$m, where e and m_e are the charge and mass of the electron, respectively, $E_{\rm rms} \equiv \langle (E^2)^{1/2}\rangle$, E and ω_L the root mean square (rms) electric field, electric field and frequency of the laser field, respectively, and c the light speed in vacuum. The temporal profile is composed by a flat-top part of $\tau_{\rm flat} = 6T_0$ and rising (falling) part of $\tau_{\rm rising\ (falling)} = 12T_0$ with Gaussian-like 5th order symmetric polynomial $10t'^3 - 15t'^4 + 6t'^5$ (here, $t' \equiv t/T_0$ and T_0 is the laser period) [27]. The number density of the gas plasma is linearly rising from $n_e = 0$ at $z = 0$ to $n_e = 1.5\times10^{18}\ {\rm cm^{-3}}$ at $z = 100\ \mu$m and then distributed uniformly to $z = 5.515$ mm. The aluminum plasma mirror is placed at $z = 5.515$ mm with a thickness of $l = 2\ \mu$m, number density $n_e = 451 n_c$ and scale length $L = \lambda_0$ for the preplasma [28], where the critical plasma density is $n_c = m_e\omega_L^2/4\pi e^2$. The spatial sizes of the simulation box are $z\times x\times y = 127\lambda_0\times 80\lambda_0\times 80\lambda_0$ with cell sizes of $4000\times256\times256$. The numbers of macro-particle per cell are assigned as 2 and 1 for electrons and Helium ions, respectively. Note that the above mentioned spatial sizes are not fine enough to resolve the plasma frequency of the aluminum target, thus the reflection of the laser pulse is recalculated with finer grid sizes of $\Delta z\times\Delta x = \frac{\lambda_0}{200}\times\frac{\lambda_0}{50}$ via the two dimensional PIC to efficiently reduce the massive 3D computation time, and, the numbers of macro-particle per cell for electrons and ions are set to 100 and 30, respectively.

Simulation results of emitted CP γ-ray beam are shown in Fig. 2. The peak intensity of emitted γ-rays is in the order of 10^7 mrad^{-1} for photon energies $\varepsilon_\gamma \geq 5$ keV. The corresponding brilliances (average helicities $\overline{h}_\gamma$) are 4.35×10^{21} (0.37), 1.37×10^{22} (−0.11), 5.89×10^{21} (−0.20) and 1.46×10^{21} (−0.21) photons/(s · mm^2 · mrad^2 · 0.1%BW) for $\varepsilon_\gamma =$ 1 MeV, 10 MeV, 100 MeV and 200 MeV, respectively. Here, the angular spread of the γ-ray beam $\Delta\theta_\gamma$ originates from the angular spread of the electron beam $\Delta\theta_e$ and the laser induced transverse momentum $p_{e,\perp} = \sqrt{p_{e,x}^2 + p_{e,y}^2} \sim a_0$, i.e., $\Delta\theta_\gamma \simeq \Delta\theta_e + 2p_{e,\perp}/p_{e,z} \simeq \Delta\theta_e + 2a_0/\overline{\gamma}_e$, where $\overline{\gamma}_e$ is the average Lorentz factor of electrons. Note that here for ultra-relativistic electrons $\gamma_e \gg 1$ the γ-photons are assumed to be emitted along the electron momentum (due to the emission solid angle $\sim 1/\gamma_e$). However, since high-energy electrons (with electron energies $\varepsilon_e \approx 900$ MeV and 1400 MeV) are concentrated in a narrow angle of less than 1 mrad, $\Delta\theta_\gamma \approx 2a_0/p_{e,z} \approx$ 3-4 mrad [see Figs. 2(a) and 3(b)]. The average helicity $\overline{h}_\gamma$ of γ-photons within a narrow cone of $\Delta\theta \lesssim 1$ mrad can reach −0.38, but for other photons of $\Delta\theta \gtrsim 3$ mrad, $\overline{h}_\gamma$ is in the range of (−0.01, 0.01) [see Fig. 2(b)]. The energy-resolved $\overline{h}_\gamma$ presents quite different feature, and can reach nearly 1.0 at low energies of ∼10 keV. $\overline{h}_\gamma$ quickly drops to ∼ −0.59 in the vicinity of 20 keV and then rises to ∼ 0.37 around 1 MeV [see Fig. 2(e)]. In

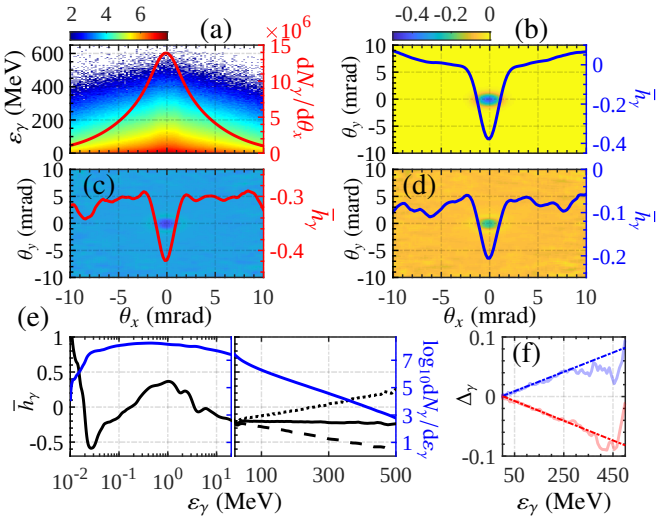


FIG. 2. (a) Number density of emitted photons $\mathrm{d}^2N_\gamma/\mathrm{d}\theta_x\mathrm{d}\varepsilon_\gamma$ (mrad^{-1} MeV^{-1}) vs deflection angle $\theta_x = p_{\gamma,x}/p_{\gamma,z}$ and γ-photon energy ε_γ. (b)-(d) Angle-resolved average helicity $\overline{h}_\gamma$ of emitted photons with unpolarized electrons (electron helicity $h_e = 0$), and, polarized electrons with $h_e = -1$ and +1, respectively. In (c) and (d), only photons with $\varepsilon_\gamma \geq 100$ MeV are taken into account. Solid lines indicate the lineout along the deflection angle $\theta_y = p_{\gamma,y}/p_{\gamma,z} = 0$ with $\Delta\theta_y = 0.12$ mrad. (e) Blue lines indicate the emission spectra $\mathrm{d}N_\gamma/\mathrm{d}\varepsilon_\gamma$ (MeV^{-1}) vs ε_γ, and black solid, dashed and dotted lines indicate $\overline{h}_\gamma$ vs ε_γ for the cases of $h_e = 0, -1$ and +1, respectively. (f) Relative deviation of energy spectra $\Delta_\gamma = 2\frac{\mathcal{N}_{\rm pol}-\mathcal{N}_{\rm unpol}}{\mathcal{N}_{\rm pol}+\mathcal{N}_{\rm unpol}}$ with $\mathcal{N} \equiv \mathrm{d}N_\gamma/\mathrm{d}\varepsilon_\gamma$, where blue and red lines indicate $h_e = +1$ and −1, respectively; solid lines are from the simulation results, and dash-dotted lines are fitting curves.

the high-energy regime $\varepsilon_\gamma \gtrsim 20$ MeV, $\overline{h}_\gamma$ saturates at $\simeq -0.2$. When employing polarized electron bunches, the radiation spectra and angular distribution are almost identical to the unpolarized case with an relative deviation of 0.9%, 1.7% and 3.3% around $\varepsilon_\gamma \approx 50, 100$ and 200 MeV, respectively [see Fig. 2(f)]. Angle-resolved $\overline{h}_\gamma$ of polarized cases also show similar patterns to that in Fig. 2(b) and consequently are excluded. For $\varepsilon_\gamma \gtrsim 100$ MeV, angle-resolved $\overline{h}_\gamma$ is in the order of −0.31 (−0.08) for $h_e = -1$ (+1) [see Figs. 3(c) and (d)]. Especially, in a narrow cone of $\Delta\theta \leq 1$ mrad, $\overline{h}_\gamma \simeq -0.42$ (−0.21) for $h_e = -1(+1)$ which means that large numbers of γ-photons with $\varepsilon_\gamma \simeq$ (20-40) keV are generated with small angular spread [see Figs. 2(c)-(e)]. Besides, for γ-photons with energies of $\varepsilon_\gamma \lesssim 20$ MeV, $\overline{h}_\gamma$ is identical to the unpolarized case. However, in the high-energy part of $\varepsilon_\gamma \gtrsim 20$ MeV, $\overline{h}_\gamma$ is linearly rising (falling) as ε_γ in the case of $h_e = +1$ (−1) and reaches $\simeq 0.25$ (−0.61) at the energy cutoff of $\varepsilon_\gamma \simeq 500$ MeV [see Fig. 2(e)]. Such brilliant CP γ-ray beam can be used for polarized lepton creation with $\varepsilon_\gamma \gtrsim 1.022$ MeV ($2m_ec^2$) [9] and photo-nuclear physics with $\varepsilon_\gamma \simeq$ 10-100 MeV [10].

The physical reasons of generating the CP γ-ray beam are analyzed in Fig. 3. In LWFA process, two plasma bubbles are excited and trap electrons [see Fig. 3(a)] to create two

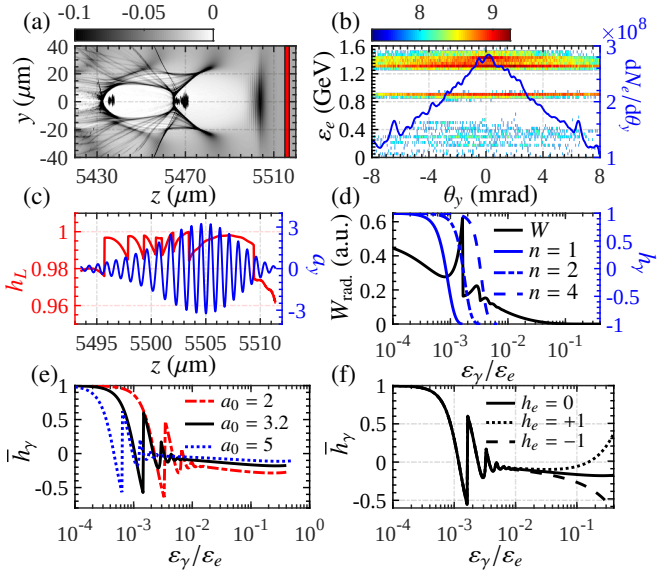


FIG. 3. (a) Number density of accelerated electrons n_e/n_c in z-y plane with $x = 0$. The red band denotes the aluminum plasma target. (b) Number distribution of electrons $\log_{10}[\mathrm{d}^2N_e/\mathrm{d}\theta_x\mathrm{d}\varepsilon_e]$ (mrad^{-1} MeV^{-1}) vs θ_x and ε_e. (c) Blue and red lines indicate the envelop and helicity of the reflected laser pulse, respectively. (d) Black solid line indicates the emission rate [normalized by W_0 in Eq. (1)] with respect to $\varepsilon_\gamma/\varepsilon_e$. Blue solid, dash-dotted and dashed lines indicate h_γ as absorbing 1, 2 and 4 photons, respectively. (e) and (f) $\bar{h}_\gamma$ vs $\varepsilon_\gamma/\varepsilon_e$ for different laser intensities and electron helicities, respectively.

isolated quasi-monoenergtic electron bunches with peak energy $\varepsilon_{e,\rm peak} \approx 900$ MeV and 1.4 GeV, respectively [see Fig. 3(b)] (similar to those in [27]). The total numbers of accelerated electrons are 4.6×10^8 (74 pC) with energy spread of 5% at $\varepsilon_{e,\rm peak} \approx 900$ MeV and 1.8×10^9 (288 pC) with energy spread of 10% at $\varepsilon_{e,\rm peak} \approx 1.4$ GeV, respectively. Angular spread of all electrons is $\Delta\theta_e \approx 12$ mard, but for high-energy electrons near $\varepsilon_{e,\rm peak} \simeq 900$ MeV (1.4 GeV), $\Delta\theta_e \simeq 1$ mrad [see Fig. 3(b)]. Due to the inhomogeneity of the electron density, the driving laser is chirped when propagating in the front of the wakefield [see the y-component of the reflected laser in Fig. 3(c)]. After reflection, due to the frequency chirping, the helicity of the driving laser is flipped and changes from negative $h_L = -1$ (right-hand rotation) to positive ~ 0.98 (left-hand rotation) (the laser helicity is calculated via $h_L = 2\mathrm{Im}(E_x^* E_y)/|E_x^* E_y|$ [26, 29], where $E_{x,y}$ are the complex amplitudes of the electric field in x and y directions, respectively, and E_x^* is the complex conjugate of E_x). Note that the deviation due to the frequency chirping is evaluated via semi-classical calculations [30] and the average relative errors in energy spectra and helicity are both only about 1.3%.

When electrons scatter with the reflected CP laser, they may absorb single or multiple low-energy laser photons and then emit a high-energy γ-photon via nonlinear Compton scattering. In the weakly nonlinear regime ($a_0 \gtrsim 1$), the polarization-dependent cross section is given by [26, 31]

$$W_{if} = W_0 \sum_{n=1}^{\infty} \int_0^{\delta_n} d\delta [F_{1n} + h_L h_e F_{2n} + h_\gamma (h_L F_{3n} + h_e F_{4n})], \quad (1)$$

with the photon helicity

$$h_\gamma = \frac{h_L F_{3n} + h_e F_{4n}}{F_{1n} + h_L h_e F_{2n}}, \quad (2)$$

where $W_0 = \frac{\alpha m_e^2 a_0^2}{4\varepsilon_{\rm eff}}$, $\alpha = 1/137$ is the fine structure constant, $\varepsilon_{\rm eff} = \varepsilon_e + a_0^2\varepsilon_L/\Lambda$ the effective energy of initial electron in the laser field, $\delta = (k_\gamma \cdot k_L)/(k_L \cdot p)$, $\delta_n = n\Lambda/(1 + a_0^2 + n\Lambda)$ the cutoff energy fraction of emitted photon absorbing n laser photons [31], $\Lambda = 2(k_L \cdot p)/m_e^2$ the laser energy parameter, p, k_L and k_γ the four-momenta of the initial electron, laser photon and emitted photon, respectively, ε_L the energy of the laser photon. F_{kn} ($k = 1, 2, 3, 4$) in Eq. (1) are given in detail in Refs. [31, 32]. In strongly nonlinear Compton scattering with $a_0 \gg 1$, the photon polarization h_γ is mainly determined by the electron helicity h_e [11, 33], however, in the weakly nonlinear regime, h_γ not only depends on the electron helicity h_e, but also on the scattering laser helicity h_L; see Eq. (2).

For unpolarized electrons ($h_e = 0$), the average helicity of emitted γ-photons via the n-photon absorption channel is given by $\bar{h}_\gamma = \frac{\sum_n F_{3n}}{\sum_n F_{1n}} h_L$. As $\varepsilon_\gamma/\varepsilon_e \sim \delta \ll \delta_1 \approx 0.0015$, the emitted photons are mainly contributed by the one-photon absorption channel ($n = 1$) and $\bar{h}_\gamma \approx 1$, i.e., the helicities of emitted γ-photons are solely determined by the laser helicity [see Fig. 3(e)]. For $10^{-3} \lesssim \delta \lesssim 7 \times 10^{-3}$, corresponding to multi-photon absorption with $1 \le n \le 5$, $\bar{h}_\gamma$ is rapidly oscillating due to the competition among different multi-photon absorption channels with significant gaps of $(\delta_n - \delta_{n-1})$ for small n [see h_γ for different channels in Fig. 3(d) and average $\bar{h}_\gamma$ in Fig. 3(e)]. For $10^{-2} \lesssim \delta \lesssim 0.4$, $\bar{h}_\gamma$ saturates to ~ -0.15 [see Fig. 3(e)]. Above theoretical analysis further confirms our simulation results in Fig. 2. For instance, in the low-energy part ($\varepsilon_\gamma \lesssim 10$ keV) with $\delta \simeq 1 \times 10^{-5} \ll \delta_1$, one obtains $\bar{h}_\gamma \approx 1$, while in the high-energy part ($\varepsilon_\gamma \gtrsim 20$ MeV) with $\delta \gtrsim 0.014$-$0.022 \gtrsim \delta_5$, $\bar{h}_\gamma$ saturates to ~ -0.21 [see Fig. 2(e)]. Moreover, since the first Compton edge (i.e., the cutoff energy of one-photon absorption channel) occurs at $\varepsilon_\gamma \simeq 1.3$-2 MeV, $\bar{h}_\gamma$ peaks around $\varepsilon_\gamma \approx 1$ MeV, and, due to the mixture of $\bar{h}_\gamma$ derived from $\varepsilon_e \approx 900$ MeV and 1.4 GeV, the valley zone of $\bar{h}_\gamma$ near $10^{-4} \lesssim \delta \lesssim \delta_1$ (10 keV $\lesssim \varepsilon_\gamma \lesssim 1$ MeV) is broadened and the fast oscillation near $10^{-3} \lesssim \delta \lesssim 10^{-2}$ (1.8 MeV $\lesssim \varepsilon_\gamma \lesssim$ 15 MeV) is smoothed [see the comparison between Fig. 2(e) and Fig. 3(e)]. Note that in the high-energy part ($\varepsilon_\gamma \gtrsim 20$ MeV) in Fig. 3(e), $\bar{h}_\gamma$ saturates to ~ -0.21 which lies between the analytical saturation values of -0.18 and -0.28 for $a_0 = 3.2$ and 2.0 [see Fig. 2(e) and Fig. 3(e)], and the slight deviation is derived from the finite-pulse effect in our numerical simulation (by comparison, we employ a monochromatic plane wave in the analytical estimation).

Furthermore, when electrons are polarized [34, 35], the impact of the electron helicity h_e on the emitted photon helicity $\bar{h}_\gamma$ is negligible in the low-energy regime of $\varepsilon_\gamma/\varepsilon_e \lesssim 10^{-2}$ [see

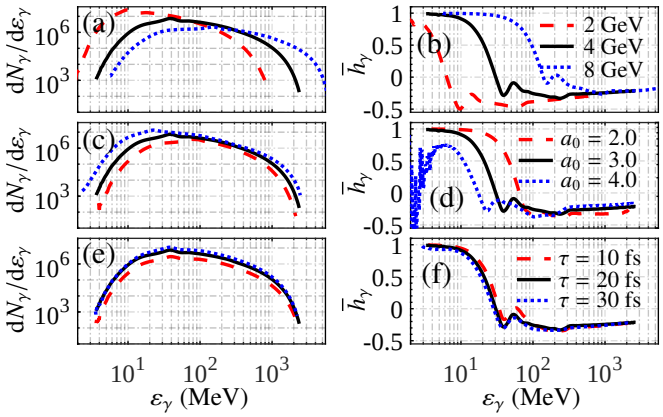


FIG. 4. Impact of [(a) and (b)] $\varepsilon_{e,\mathrm{peak}}$, [(c) and (d)] a_0, [(e) and (f)] laser pulse duration τ on $\bar{h}_\gamma$. Other parameters are the follows: for the electrons $\varepsilon_{e,\mathrm{peak}} = 4$ GeV, energy spread 3%, $\Delta\theta_e = 0.2$ mrad, transverse beam size $\sigma_t = 2.1$ μm, beam length $l_e = 5$ μm and total charge 300 pC; for the driving laser, the spatial profile is Gaussian with $a_0 = 3.0$, $\tau = 20$ fs and transverse focal radius $w_0 = 11$ μm.

Fig. 2(e) and Fig. 3(f)]. However, as $\varepsilon_\gamma/\varepsilon_e \gtrsim 10^{-2}$, $\bar{h}_\gamma$ will linearly increase (decrease) for $h_e = +1$ (-1) [see Fig. 3(f)]. This analytical tendency completely coincides with our numerical results in Fig. 2(e).

For the experimental feasibility, the impact of the laser and plasma parameters on $\bar{h}_\gamma$ is analyzed in Fig. 4. In the LWFA process, the peak energy of accelerated electrons $\varepsilon_{e,\mathrm{peak}}$ scales with the laser power P and plasma density n_e via $\varepsilon_e \propto P^{1/3} n_e^{-2/3} \lambda_0^{-4/3}$ [27]. Thus, in Figs. 4(a) and (b), the impact of n_e is simulated via $\varepsilon_e \propto n_e^{-2/3}$ with $\varepsilon_{e,\mathrm{peak}} = 2, 4,$ and 8 GeV corresponding to $n_e = 8.8 \times 10^{17}$, 3.1×10^{17} and 1.1×10^{17} cm^{-3}, respectively. As the emission rate $W_0 \propto 1/\varepsilon_{e,\mathrm{eff.}} \propto 1/\varepsilon_e$ [see Eq. (1)], lower (higher) energies of incident electrons will induce higher (lower) yields [see Fig. 4(a)]. Since the n-photon absorption cutoff $\varepsilon_{\gamma,\mathrm{cutoff}} = \delta_n \varepsilon_e$ will shift due to the variation of electron energy (but the shift in δ_n is quite small), the energy spectra in Fig. 4(a) and $\bar{h}_\gamma$ in Fig. 4(b) will shift to left (right) as increasing (decreasing) the electron energy. But, the final saturation $\bar{h}_\gamma \simeq -0.2$ remains unchanged [see Fig. 4(b)]. The laser intensity a_0 will affect both the emission probability and the nonlinearity of scattering process. As $W_0 \propto a_0^2$, the radiation intensity will increase (decrease) for smaller (larger) a_0 [see Fig. 4(c)]. For larger a_0, δ_n will be smaller, thus, $\bar{h}_\gamma$ will shift to left, and vice versa [see Fig. 4(d)]. In addition, increasing (decreasing) the laser pulse τ will yield more (fewer) photons per electron [see Fig. 4(e)]. However, due to short pulse effect (average a_0 will be lower for shorter pulse), $|\bar{h}_\gamma|$ is slight higher for $\tau = 10$ fs than $\tau = 20$ fs and 30 fs [see Fig. 4(f)].

In conclusion, we put forward an efficient brilliant CP γ-rays generation method via single-shot laser plasma interaction. We find that in the weakly nonlinear regime of Compton scattering, the helicity of emitted photon is subjected to the interplay of the laser and electron helicities. Our proposed method can generate γ-photons with peak brilliance of 10^{21}-10^{22} photons/(s $\cdot$ mm^2 $\cdot$ mrad^2 $\cdot$ 0.1%BW) and average polarization degree of $\sim$ 21%-37% with moderate laser pulses. Moreover, our method is quite stable in a wide range of laser and plasma parameters. With proper selection of γ-photon energy and (polarized) plasma target, highly CP brilliant γ-ray sources can be obtained for many applications, such as, photonuclear researches, generation of polarized lepton sources, etc.

ACKNOWLEDGEMENTS

This work is supported by the National Natural Science Foundation of China (Grants Nos. 11905169, 12022506, 11874295), and the China Postdoctoral Science Foundation (Grant No. 2020M683447).

[1] A. J. Dean, D. J. Clark, J. B. Stephen, V. A. McBride, L. Bassani, A. Bazzano, A. J. Bird, A. B. Hill, S. E. Shaw, and P. Ubertini, Polarized gamma-ray emission from the Crab, Science **321**, 1183 (2008).

[2] R. Bühler and R. Blandford, The surprising Crab pulsar and its nebula: A review, Rept. Prog. Phys. **77**, 066901 (2014), arXiv:1309.7046 [astro-ph.HE].

[3] E. Orlando and A. Strong, Galactic synchrotron emission with cosmic ray propagation models, Mon. Not. Roy. Astron. Soc. **436**, 2127 (2013), 1309.2947 [astro-ph.GA].

[4] H. R. Weller and M. W. Ahmed, The HIγS Facility: A free-electron laser generated gamma-ray beam for research in nuclear physics, Modern Physics Letters A **18**, 1569 (2003).

[5] H. R. Weller, M. W. Ahmed, H. Gao, W. Tornow, Y. K. Wu, M. Gai, and R. Miskimen, Research opportunities at the upgraded hiγs facility, Progress in Particle and Nuclear Physics **62**, 257 (2009).

[6] L. Schoeffel, C. Baldenegro, H. Hamdaoui, S. Hassani, C. Royon, and M. Saimpert, Photon–photon physics at the LHC and laser beam experiments, present and future, Prog. Part. Nucl. Phys. **120**, 103889 (2021), arXiv:2010.07855 [hep-ph].

[7] R. W. Assmann et al., EuPRAXIA Conceptual Design Report, Eur. Phys. J. ST **229**, 3675 (2020), [Erratum: Eur. Phys. J. ST 229, 11–31 (2020)].

[8] T. Omori, M. Fukuda, T. Hirose, Y. Kurihara, R. Kuroda, M. Nomura, A. Ohashi, T. Okugi, K. Sakaue, T. Saito, J. Urakawa, M. Washio, and I. Yamazaki, Efficient propagation of polarization from laser photons to positrons through compton scattering and electron-positron pair creation, Phys. Rev. Lett. **96**, 114801 (2006).

[9] G. Moortgat-Pick and et.al., Polarized positrons and electrons at the linear collider, Physics Reports **460**, 131 (2008).

[10] J. Speth and A. van der Woude, Giant resonances in nuclei, Reports on Progress in Physics **44**, 719 (1981).

[11] Y.-F. Li, R. Shaisultanov, Y.-Y. Chen, F. Wan, K. Z. Hatsagortsyan, C. H. Keitel, and J.-X. Li, Polarized ultrashort brilliant multi-gev γ rays via single-shot laser-electron interaction, Phys. Rev. Lett. **124**, 014801 (2020).

[12] C. Schaerf, Polarized gamma-ray beams, Physics Today **58**, 44 (2005),.

[13] C. N. Danson, C. Haefner, J. Bromage, T. Butcher, J.-C. F. Chanteloup, E. A. Chowdhury, A. Galvanauskas, L. A. Gizzi, J. Hein, D. I. Hillier, N. W. Hopps, Y. Kato, E. A. Khazanov, R. Kodama, G. Korn, R. Li, Y. Li, J. Limpert, J. Ma, C. H. Nam, D. Neely, D. Papadopoulos, R. R. Penman, L. Qian, J. J. Rocca, A. A. Shaykin, C. W. Siders, C. Spindloe, S. Szatmári, R. M. G. M. Trines, J. Zhu, P. Zhu, and J. D. Zuegel, Petawatt and exawatt class lasers worldwide, High Power Laser Sci. Eng. **7**, e54 (2019).

[14] J. W. Yoon, Y. G. Kim, I. W. Choi, J. H. Sung, H. W. Lee, S. K. Lee, and C. H. Nam, Realization of laser intensity over 10^{23} W/cm^2, Optica **8**, 630 (2021).

[15] E. Esarey, C. B. Schroeder, and W. P. Leemans, Physics of laser-driven plasma-based electron accelerators, Rev. Mod. Phys. **81**, 1229 (2009).

[16] A. Macchi, M. Borghesi, and M. Passoni, Ion acceleration by superintense laser-plasma interaction, Rev. Mod. Phys. **85**, 751 (2013).

[17] S. Corde, K. Ta Phuoc, G. Lambert, R. Fitour, V. Malka, A. Rousse, A. Beck, and E. Lefebvre, Femtosecond x rays from laser-plasma accelerators, Rev. Mod. Phys. **85**, 1 (2013).

[18] G. Sarri, D. J. Corvan, W. Schumaker, J. M. Cole, A. Di Piazza, H. Ahmed, C. Harvey, C. H. Keitel, K. Krushelnick, S. P. D. Mangles, Z. Najmudin, D. Symes, A. G. R. Thomas, M. Yeung, Z. Zhao, and M. Zepf, Ultrahigh brilliance multi-mev γ-ray beams from nonlinear relativistic thomson scattering, Phys. Rev. Lett. **113**, 224801 (2014).

[19] W. Yan, C. Fruhling, G. Golovin, D. Haden, J. Luo, P. Zhang, B. Zhao, J. Zhang, C. Liu, M. Chen, S. Chen, S. Banerjee, and D. Umstadter, High-order multiphoton thomson scattering, Nature Photonics **11**, 514 (2017).

[20] C. P. Ridgers, C. S. Brady, R. Duclous, J. G. Kirk, K. Bennett, T. D. Arber, A. P. L. Robinson, and A. R. Bell, Dense electron-positron plasmas and ultraintense γ rays from laser-irradiated solids, Phys. Rev. Lett. **108**, 165006 (2012).

[21] X.-L. Zhu, M. Chen, S.-M. Weng, T.-P. Yu, W.-M. Wang, F. He, Z.-M. Sheng, P. McKenna, D. A. Jaroszynski, and J. Zhang, Extremely brilliant gev γ-rays from a two-stage laser-plasma accelerator, Science Advances **6**, eaaz7240 (2020),.

[22] K. Xue, Z.-K. Dou, F. Wan, T.-P. Yu, W.-M. Wang, J.-R. Ren, Q. Zhao, Y.-T. Zhao, Z.-F. Xu, and J.-X. Li, Generation of highly-polarized high-energy brilliant γ-rays via laser-plasma interaction, Matter and Radiation at Extremes **5**, 054402 (2020).

[23] B. King and S. Tang, Nonlinear compton scattering of polarized photons in plane-wave backgrounds, Phys. Rev. A **102**, 022809 (2020).

[24] K. T. Phuoc, S. Corde, C. Thaury, V. Malka, A. Tafzi, J. P. Goddet, R. C. Shah, S. Sebban, and A. Rousse, All-optical compton gamma-ray source, Nat. Photonics **6**, 308 (2012).

[25] T. D. Arber, K. Bennett, C. S. Brady, A. Lawrence-Douglas, M. G. Ramsay, N. J. Sircombe, P. Gillies, R. G. Evans, H. Schmitz, A. R. Bell, and C. P. Ridgers, Contemporary particle-in-cell approach to laser-plasma modelling, Plasma Phys. Control. Fusion **57**, 113001 (2015).

[26] K. Yokoya, CAIN 2.42 User Manual.

[27] W. Lu, M. Tzoufras, C. Joshi, F. S. Tsung, W. B. Mori, J. Vieira, R. A. Fonseca, and L. O. Silva, Generating multi-gev electron bunches using single stage laser wakefield acceleration in a 3d nonlinear regime, Phys. Rev. ST Accel. Beams **10**, 061301 (2007).

[28] T. Z. Esirkepov, J. K. Koga, A. Sunahara, T. Morita, M. Nishikino, K. Kageyama, H. Nagatomo, K. Nishihara, A. Sagisaka, H. Kotaki, T. Nakamura, Y. Fukuda, H. Okada, A. S. Pirozhkov, A. Yogo, M. Nishiuchi, H. Kiriyama, K. Kondo, M. Kando, and S. V. Bulanov, Prepulse and amplified spontaneous emission effects on the interaction of a petawatt class laser with thin solid targets, Nuclear Instruments and Methods in Physics Research Section A: Accelerators, Spectrometers, Detectors and Associated Equipment **745**, 150 (2014).

[29] B. E. A. Saleh and M. C. Teich, Fundamentals of Photonics (Wiley, 1991).

[30] T. N. Wistisen and A. Di Piazza, Numerical approach to the semiclassical method of radiation emission for arbitrary electron spin and photon polarization, Phys. Rev. D **100**, 116001 (2019).

[31] Y. S. Tsai, Laser + $e^- \to \gamma + e^-$ and laser + $\gamma \to e^+ + e^-$ as sources of producing circularly polarized γ and $e^\pm$ beams, Phys. Rev. D **48**, 96 (1993).

[32] D. Y. Ivanov, G. L. Kotkin, and V. G. Serbo, Complete description of polarization effects in emission of a photon by an electron in the field of a strong laser wave, Eur. Phys. J. C **36**, 127 (2004).

[33] V. N. Baier, V. M. Katkov, and V. M. Strakhovenko, Electromagnetic Processes at High Energies in Oriented Single Crystals (World Scientific, Singapore, 1998).

[34] M. Wen, M. Tamburini, and C. H. Keitel, Polarized laser-wakefield-accelerated kiloampere electron beams, Phys. Rev. Lett. **122**, 214801 (2019).

[35] Z. Nie, F. Li, F. Morales, S. Patchkovskii, O. Smirnova, W. An, N. Nambu, D. Matteo, K. A. Marsh, F. Tsung, W. B. Mori, and C. Joshi, In situ generation of high-energy spin-polarized electrons in a beam-driven plasma wakefield accelerator, Phys. Rev. Lett. **126**, 054801 (2021).